

WARP Logic Neural Networks

Lino Gerlach ^{*1} Thore Gerlach ^{*2} Liv Våge ¹ Elliott Kauffman ¹ Isobel Ojalvo ¹

Abstract

Fast and efficient AI inference is increasingly important, and recent models that directly learn low-level logic operations have achieved state-of-the-art performance. However, existing logic neural networks incur high training costs, introduce redundancy or rely on approximate gradients, which limits scalability. To overcome these limitations, we introduce WAlsh Relaxation for Probabilistic (WARP) logic neural networks—a novel gradient-based framework that efficiently learns combinations of hardware-native logic blocks. We show that WARP yields the most parameter-efficient representation for exactly learning Boolean functions and that several prior approaches arise as restricted special cases. Training is improved by introducing learnable thresholding and residual initialization, while we bridge the gap between relaxed training and discrete logic inference through stochastic smoothing. Experiments demonstrate faster convergence than state-of-the-art baselines, while scaling effectively to deeper architectures and logic functions with higher input arity.

1. Introduction

Deep learning (LeCun et al., 2015) has become the standard for a wide range of tasks in science, but its success comes with heavy computational costs in both training and inference. This restricts deployability in many real-world settings—particularly in domains where ultra-fast inference is critical, such as healthcare (Bacellar et al., 2025), particle physics (Arrestad et al., 2021), gravitational wave astronomy (Martins et al., 2025), and quantum computing (Bhat et al., 2025). These constraints have motivated substantial research into the development of models that maintain predictive accuracy while improving computational efficiency.

^{*}Equal contribution ¹Princeton University ²European Space Agency, Advanced Concepts Team. Correspondence to: Lino Gerlach <lg0508@princeton.edu>, Thore Gerlach <thore.gerlach@esa.int>.

Prominent among such efforts are model compression techniques, which encompass approaches for inducing sparsity (Sung et al., 2021; Hoefer et al., 2021), pruning (Lin et al., 2018; Liu et al., 2022), and reducing numerical precision via weight quantization (Sun et al., 2024; Gholami et al., 2022; Chmiel et al., 2021).

Nevertheless, such approaches do not directly address the intrinsic computational cost of numerical multiplication. To overcome this limitation, multiplication-free architectures have been proposed, including binary neural networks (Hubara et al., 2016; Qin et al., 2020) and other bit-level summation models (Chen et al., 2020; Elhoushi et al., 2021; Nguyen et al., 2024). However, efficient inference on digital hardware requires mapping abstract computations into executable logic, which incurs significant overhead.

Within the domain of multiplication-free models, Logic Neural Networks (LNNs), also denoted as Weightless Neural Networks (WNNs) (Aleksander et al., 2009), represent a distinct class that overcomes this limitation. Instead of relying on weighted connections, LNNs employ binary look-up tables (LUTs) or logic gates to drive neural activity during inference, allowing them to capture highly nonlinear behaviors while avoiding arithmetic operations altogether. Although state-of-the-art models achieve remarkable performance on small-scale tasks, their scalability remains constrained—whether due to limited expressiveness (Susskind et al., 2023; Andronic & Constantinides, 2023), reliance on gradient approximations (Bacellar et al., 2024), double-exponential growth in parameter requirements (Petersen et al., 2022; 2024), or large discretization gaps (Kim, 2023; Yousefi et al., 2025), describing an accuracy mismatch between the training using relaxations and discrete inference. We overcome these issues by proposing WAlsh Relaxation for Probabilistic (WARP) LNNs, based on differentiable relaxation, similar to Differentiable Logic Gate Networks (DLGN) (Petersen et al., 2022). We propose representing Boolean functions with the Walsh–Hadamard (WH) transform (Kunz, 1979), providing a compact and differentiable parameterization of a deep LNN enabling an exponential reduction in the number of parameters compared to DLGNs. Publishing our code will bridge the gap created by the lack of publicly available convolutional DLGN implementations for the community. Our key contributions, depicted in Fig. 1, are summarized as follows:

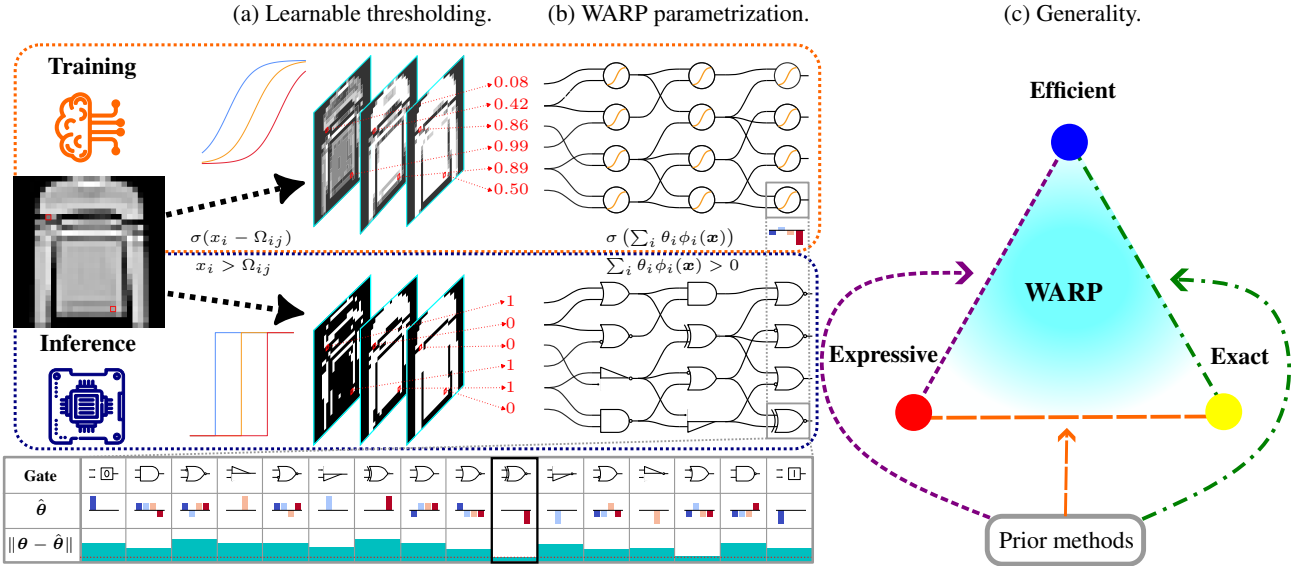


Figure 1. Overview of proposed WARP LNNs enabling differentiable learning of Boolean functions. During training, single neurons are continuously relaxed, while being replaced by a logic function to enable fast and efficient inference. **(a)** We propose learnable thresholding with relaxing input binarization, which leads to improved performance. **(b)** For parameterizing neurons, we introduce WARP which is based on the Walsh-Hadamard transform. This leads to exponentially less parameters (16 to 4 for $n = 2$) and deployable logic structures are obtained by optimal thresholding. **(c)** WARP is maximally parameter-efficient, does not rely on approximate gradients (exact) and is fully expressive, describing the ability to represent any Boolean function (see Theorem 4.1). While previous methods mostly satisfy only two of these properties (parameter inefficient (Petersen et al., 2022), inexact through approximations (Bacellar et al., 2024) or not fully expressive (Hoang et al., 2025; Andronic & Constantinides, 2025)), they can be deduced from WARP as special cases.

- **WARP Parametrization:** We propose WARP-LNNs, utilizing a new differentiable relaxation of higher-input Boolean functions. This does not only increases expressiveness over DLGNs, but also reduces the number of parameters exponentially. Through residual initialization and stochastic smoothing, we enable fast convergence, stable gradients and improve discrete inference accuracy.
- **Representation Generality:** We show that WARP is the most general and efficient parametrization for representing Boolean functions maintaining full expressiveness. We shed light on the interconnections between state-of-the-art models from the literature and show that they are deduced by basis changes, weight restrictions, approximative gradients or non-invertible input mappings.
- **Learnable Thresholding:** For LNNs, data has to be binarized in inference. While previous methods use data-based binarization, we propose to a differentiable relaxation to enable learning the thresholds during training.
- **Experimental Effectiveness:** We demonstrate versatility across diverse settings: WARP reliably learns higher-input LUTs in deep architectures where prior SOTA methods struggle, integrates seamlessly with existing approaches to reduce the number of operations in convolutions, and leverages learnable thresholding to substantially lower the required bit precision at inference time.

2. Related Work

TreeLUT (Khataei & Bazargan, 2025) combines gradient-boosted trees with LUT mappings for efficient inference. For the remainder of this section, however, we will focus on depth-scalable LNNs.

Function Approximation Early work on LNNs explored single-layered perceptrons for approximating LUTs, enabling extremely efficient inference (Susskind et al., 2022; 2023). However, an n -input LUT has a known VC-dimension of 2^n (Carneiro et al., 2019), while a single-layered perceptron with n inputs has a VC-dimension of $n + 1$, limiting expressiveness. Although extensions to higher-degree polynomial basis (Andronic & Constantinides, 2023) and multi-layer perceptrons (Andronic & Constantinides, 2024; 2025; Weng et al., 2025; Hoang et al., 2025) have been proposed, these models fall short on expressivity and are faced with exponential training complexity.

Linear Combination To address these limitations, DLGNs utilize differentiable relaxations of logic gates, enabling gradient-based training of multi-layer architectures (Petersen et al., 2022; 2024). Advances in connection learning (Mommen et al., 2025; Yue & Jha, 2024; Kresse et al., 2025) have improved flexibility, but training DLGNs introduces a discretization gap between training and discrete

inference. Recent work has sought to bridge this gap by stochastic relaxation (Kim, 2023; Yousefi et al., 2025).

Direct Parametrization DLGNs remain restricted to two-input gates and suffer from double-exponential parameter growth, limiting scalability. To account for higher-degree LUTs, the authors of (Bacellar et al., 2024) propose Differentiable WNNs (DWNs) to directly parametrize LUTs, leading to a logarithmic parameter reduction compared to DLGNs. For obtaining differentiability, the addressing function is relaxed to continuous values and gradients are approximated, degrading performance for deep models.

Basis Parametrization Recently, alternative parametrization schemes for representing Boolean functions have been developed (Rüttgers et al., 2025; Ramírez et al., 2025). While overcoming the restrictions of double-exponentially many parameters from DLGNs and approximative gradients of DWNs, these methods still suffer from large discretization errors. This leads to instability in weight initialization and vanishing gradients.

3. Background

Before we propose our reparametrization scheme for Boolean functions in Sec. 4, we begin by reviewing fully expressive LNN approaches from the literature and highlight their limitations. For the remainder of this paper, we fix the following notation. Matrices/vectors are denoted by upper/lower case letters, e.g., A/a , and we denote the binary representation of integer i with $\mathbf{b}^{(i)} \in \{0, 1\}^n$ starting with the least significant bit, $n = \lceil \log_2 i \rceil$. Further, let $[n] = \{1, \dots, n\}$, $\sigma(\cdot)$ represent the sigmoid function, $\mathbb{1}$ the indicator function, and $\mathbf{t}^{(f)} \in \{0, 1\}^{2^n}$ the LUT of a function $f : \{0, 1\}^n \rightarrow \{0, 1\}$. Finally, let $\varphi : \{0, 1\} \rightarrow \{-1, 1\}$ denote the bijection $\varphi(x) = 1 - 2x$.

3.1. Differentiable Logic Gate Networks

Networks composed of logical operations offer a discrete and interpretable framework for computation, but directly optimizing their combinational structure is computationally intractable due to the exponential search space. To enable efficient gradient-based optimization, prior work introduces Differentiable Logic Gate Networks (DLGNs) by relaxing discrete gate assignments into a continuous, trainable parametrization (Petersen et al., 2022; 2024).

Parametrization DLGNs find the ideal combination of gates by calculating a weighted sum over all possible gates at each node of the computational graph and calculating a gradient w.r.t. these weights. The approach involves continuously relaxing onto the simplex spanning all possible

Boolean functions:

$$f_{\text{DLGN}}(\mathbf{x}) = \sum_{i \in [2^{2^n}]} \alpha_i \phi_i^{\text{DLGN}}(\mathbf{x}), \quad \sum_{i \in [2^{2^n}]} \alpha_i = 1, \quad (1)$$

with $\alpha_i \geq 0$ and $\phi_i^{\text{DLGN}} : \mathbb{R}^n \rightarrow [0, 1]$ being a probabilistic surrogate of the corresponding Boolean function in form of a multilinear polynomial (see Tab. 3 for the example $n = 2$). A surrogate formulation is required to accommodate real-valued inputs during training, as the underlying discrete functions are not defined in this domain. To ensure staying in the probability simplex, a softmax distribution is used for the weights in Eq. (1), i.e., $\alpha_i = \sigma(\alpha'_i) / \sum_j \sigma(\alpha'_j)$, $\alpha'_i \in \mathbb{R}$.

Limitations Originally developed for two-input logic gates, this approach can be extended to n -ary Boolean functions. However, a fundamental limitation of this approach lies in the double-exponential growth of complexity with increasing neuron arity: a single 6-input Boolean function, for example, would require $2^{2^6} = 1.8447 \cdot 10^{19}$ parameters, making the architecture computationally intractable. Consequently, DLGNs are effectively constrained to learning logic gates with very few inputs, as handling parameters per gate becomes rapidly infeasible as n increases.

During inference, all softmax operations are replaced by argmax selections, effectively rounding each neuron to the binary gate associated with the largest weight. The resulting logic gate circuit can be directly embedded in hardware such as FPGAs or ASICs for highly efficient execution. A key limitation of DLGNs is the misalignment between training and inference. Furthermore, the presence of redundancy introduces ambiguity (Rüttgers et al., 2025).

3.2. Differentiable Weightless Neural Networks

To overcome the limitation of having double-exponentially many parameters per neuron, the authors of (Bacellar et al., 2024) propose Differentiable WNNs (DWNs) by

$$f_{\text{DWN}}(\mathbf{x}) = \sum_{i \in [2^n]} \beta_i \mathbb{1}_{\mathbf{b}^{(i)}}(\varphi^{-1}(\text{sgn}(\mathbf{x}))) = \beta_j, \quad (2)$$

where j corresponds to the index where the argument of $\varphi^{-1}(\text{sgn}(\mathbf{x})) = \mathbf{b}^{(j)}$. Notably, DWNs have no restrictions on the weights, i.e., $\beta \in \mathbb{R}^{2^n}$, and thus propagate arbitrary real vectors $\mathbf{x} \in \mathbb{R}^n$ through the network.

Limitations DWNs have the problem of a non-differentiable parametrization, since the input of the previous layer is discretized to the nearest address for accessing the LUT parameters β_i . This issue is approached by using an extended finite difference method which accounts for variations in the addressed position. However, this is an inaccurate approximation and leads to training instabilities for deep models (see Sec. 5). For discrete inference, the LUTs are obtained by $t_i^{(f_{\text{DWN}})} = \varphi^{-1}(\text{sgn}(\beta_i))$.

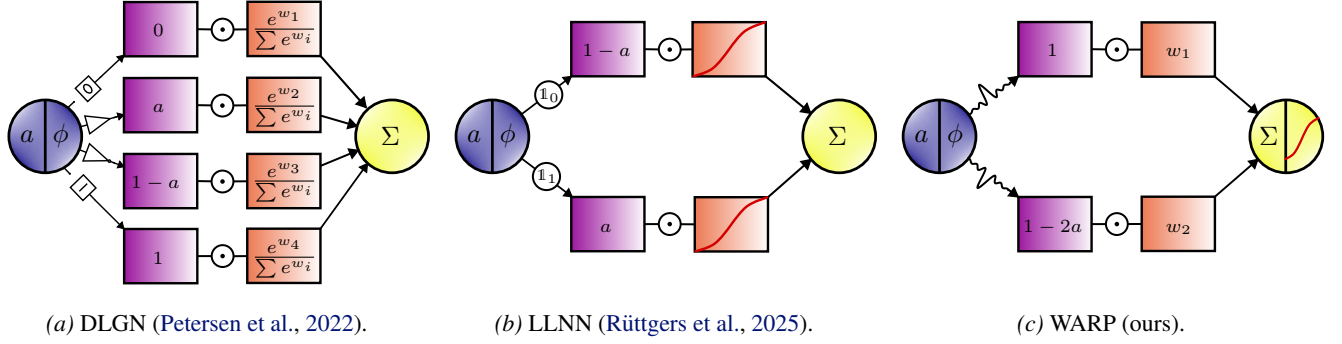


Figure 2. Our parametrization compared to methods from the literature for $n = 1$. The S-shaped curve indicates the sigmoid function.

3.3. Light Logic Neural Networks

To overcome non-differentiability, the authors of (Rüttgers et al., 2025) and (Ramírez et al., 2025) independently developed similar parametrizations. While (Ramírez et al., 2025) denote their approach as LUT LNNs (LLNNs), (Rüttgers et al., 2025) uses the term Light DLGNs (LIGHT). It uses that every n -ary Boolean function can be written as

$$f_{\text{LLNN}}(\mathbf{x}) = \sum_{i \in [2^n]} \gamma_i \phi_i^{\mathbb{1}}(\mathbf{x}), \quad \gamma_i \in [0, 1], \quad (3)$$

where $\phi_i^{\mathbb{1}}$ are indicator polynomials of the form

$$\phi_i^{\mathbb{1}}(\mathbf{x}) = \prod_{k \in [n]} x_k^{b_k^{(i)}} (1 - x_k)^{1 - b_k^{(i)}}. \quad (4)$$

Since $\phi_i^{\mathbb{1}}(\mathbf{x}) = \mathbb{1}_{b^{(i)}}(\mathbf{x})$ for $\mathbf{x} \in \{0, 1\}^n$, the Boolean functions are obtained at the corner points of the hypercube $\gamma \in \{0, 1\}^n$. $\gamma_i \in [0, 1]$ is enforced by using the sigmoid function on arbitrary real weights, i.e., $\gamma_i = \sigma(\gamma'_i)$, $\gamma'_i \in \mathbb{R}$.

Limitations Even though this reparametrization greatly reduces the number of parameters per neuron, the weight parameters in Eq. (3) are restricted to the interval $[0, 1]$. This leads to undesirable effects in the optimization landscape, resulting in vanishing gradients (Rüttgers et al., 2025).

After training, LLNNs discretize neurons into LUTs by $t_i^{(f_{\text{LLNN}})} = \varphi^{-1}(\text{sgn}(\varphi(\beta_i)))$. Small perturbations in the parameter space—especially in sharp loss landscapes—can cause significant shifts in behavior, as the selected LUT may not reflect the neuron’s actual functional output. This can lead to a large discretization gap, heavily degrading inference performance after training.

4. WARP Logic Neural Networks

For the analysis of Boolean functions—such as investigating spectral concentration (O’Donnell, 2014) and learnability (Hellerstein & Servedio, 2007)—one often considers the

symmetrical hypercube $\{-1, 1\}^n$ as domain instead, that is functions of the form $g : \{-1, 1\}^n \rightarrow \{-1, 1\}$.

4.1. Walsh–Hadamard Transform

A helpful tool for the analysis is the *Fourier expansion*

$$g(\mathbf{s}) = \sum_{i \in [2^n]} \theta_i \phi_i^{\text{W}}(\mathbf{s}), \quad \phi_i^{\text{W}}(\mathbf{s}) = \prod_{k \in [n]} s_k^{b_k^{(i)}}. \quad (5)$$

The functions ϕ_i^{W} form an orthonormal basis for all functions over $\{-1, 1\}^n$. This is also known as the *Walsh–Hadamard* (WH) transform and θ_i can be written as

$$\theta_i = \frac{1}{\sqrt{2^n}} \sum_{\mathbf{s}} g(\mathbf{s}) \phi_i^{\text{W}}(\mathbf{s}) = \frac{1}{\sqrt{2^n}} \sum_{j \in [2^n]} H_{ij} t_j^{(g)}, \quad (6)$$

where \mathbf{H} denotes the n -Hadamard matrix (Hedayat & Wallis, 1978). The spectral regularization for DWNs exactly corresponds to \mathcal{L}_2 -regularization of the parameters θ .

Intuitively, this expansion uses simple polynomial basis functions—individual variables, pairwise products, and higher-order interactions—to capture the structure of the Boolean function. Hence the WH representation provides a compressed and structured parametrization of Boolean functions, where the 2^{2^n} Boolean functions are in bijection with a finite subset of the 2^n -dimensional lattice.

Example In the special case of two inputs $\mathbf{s} = (u, v) \in \{-1, 1\}^2$, every function $g : \{-1, 1\}^2 \rightarrow \{-1, 1\}$ admits a decomposition with only four coefficients:

$$g(u, v) = \text{sgn}(\theta_1 + \theta_2 u + \theta_3 v + \theta_4(u \cdot v)),$$

where θ_1 encodes the constant bias (tendency toward $+1$ or -1), θ_2 and θ_3 encode dependence on the individual inputs, and θ_4 encodes the interaction term between the inputs. For example, the coefficients $(\theta_1, \theta_2, \theta_3, \theta_4) = (0, 0, 0, 1)$ correspond to the XOR gate, while the AND gate can be expressed as $(\theta_1, \theta_2, \theta_3, \theta_4) = (-\frac{1}{2}, \frac{1}{2}, \frac{1}{2}, \frac{1}{2})$ (see Tab. 3 for the full list of gates and coefficients for $n = 2$).

4.2. Parametrization

Instead of being restricted to the binary domain $\{-1, 1\}^n$, the WH transform in Eq. (5) decomposes an arbitrary input vector into a superposition of basis functions. This provides a differentiable relaxation for Boolean functions

$$f_{\text{WARP}}(\mathbf{x}) = \sigma \left(\frac{1}{\tau} \sum_{i \in [2^n]} \theta_i \phi_i^{\text{W}}(\varphi(\mathbf{x})) \right). \quad (7)$$

Theorem 4.1. *The WARP parametrization is the most parameter-efficient representation of any boolean function and previous approaches are special cases that either introduce redundancy (DLGN), errors through approximation (DWN) or restrictions on parameters (LLNN and LIGHT).*

The proof can be found in Sec. A. The decomposition in Eq. (7) provides a compact and differentiable parameterization with 2^n parameters, while still allowing to collapse back into one of the 2^{2^n} exact Boolean functions at inference time by choosing the closest LUT:

$$t_i^{(f_{\text{WARP}})} = \varphi^{-1} \left(\operatorname{sgn} \left(\sum_j H_{ij} \theta_j \right) \right). \quad (8)$$

Exploiting the recursive structure of \mathbf{H} , the WH transform in Eq. (8) is efficiently computable in $\mathcal{O}(n2^n)$ (Fino & Algazi, 1976). Further, this discretization is also optimal.

Theorem 4.2. *Under the WARP parametrization, the discretization that minimizes the error in any \mathcal{L}_p -norm is achieved by applying (8), or equivalently by choosing the LUT whose Walsh–Hadamard coefficients are closest to θ .*

The proof can be found in Sec. B. Note that our parametrization in Eq. (7) has three key differences compared to LIGHT in Eq. (3): (i) The removal of weight constraints prevents instability during initialization and can exacerbate vanishing gradient phenomena, (ii) nonlinearities are introduced explicitly through the sigmoid activation in contrast to LIGHT, where nonlinear dependence on the input is encoded implicitly by polynomial basis expansions, and (iii) a continuous, hyperparameter τ is incorporated, enabling additional flexibility in shaping the representation. Moreover, we introduce stochastic smoothing and residual initialization for stabilizing continuous training and improving discrete inference.

Stochastic Smoothing Using the discretization in Eq. (8), we face the same issues as for LLNN. In sharp loss regions, small parameter changes misalign LUT selections, leading to a large discretization gap and poor inference performance.

For mitigating this effect, we note that the sigmoid function characterizes a Bernoulli distribution, representing the probability of an input vector being discretized to a binary output, i.e., $\mathbb{P}(t_i^{(f_{\text{WARP}})} = 1) = f_{\text{WARP}}(\mathbf{b}^{(i)})$. To introduce stochasticity into the training process, we adopt Gumbel–Sigmoid

reparameterization, a binary variant of the Gumbel–Softmax (Concrete) distribution, enabling gradient-based training with discrete variables (Maddison et al., 2017; Jang et al., 2017). Differentiable samples $z(\mathbf{x}) \sim \text{Ber}(f_{\text{WARP}}(\mathbf{x}))$ are obtained by sampling $G_1, G_2 \sim \text{Gumbel}(0, 1)$

$$z(\mathbf{x}) = \sigma \left(\frac{1}{\tau} \sum_{i \in [2^n]} \theta_i \phi_i^{\text{W}}(\varphi(\mathbf{x})) + G_1 - G_2 \right), \quad (9)$$

with temperature parameter τ . Lower values of τ yield a tighter relaxation towards the discrete domain $\{0, 1\}$, thereby reducing the discretization gap. However, choosing τ too small can lead to numerical instabilities such as exploding gradients. In our experiments, we evaluate the performance of using discretization already during training in the forward pass as a straight-through estimator (see Sec. 5).

Residual Initialization To avoid vanishing gradients and achieving a reduced discretization gap, the authors of (Petersen et al., 2024) propose to use *residual initialization* (RI). Inspired by residual connections (He et al., 2016), a large initial probability is assigned to the pass-through function of a single input variable, e.g., $f(\mathbf{x}) = x_n$. Similarly to DLGNs, this initialization is straight-forward for WARP for a chosen probability p to the pass-through function.

$$\theta_{2^{n-1}+1} = \tau \sigma^{-1}(p), \quad \theta_i = 0, \quad \forall i \neq 2^{n-1} + 1. \quad (10)$$

A proof can be found in Sec. C in the appendix.

4.3. Learnable Thresholding

Since we learn a Boolean function for inference, data has to be binarized for compatibility, usually done by thermometer thresholding. Given a threshold matrix $\Omega \in \mathbb{R}^{l \times d}$, a data point $\mathbf{x} \in \mathbb{R}^d$ is binarized by checking $\omega_{ij} \leq x_j$. State-of-the-art examples include uniform (Petersen et al., 2024) and distributive (Bacellar et al., 2024) thresholding.

Instead of only including data-specific information, we propose to include information on the given task by learning the matrix Ω simultaneously with the network parameters. For thermometer thresholding, the row entries have to be monotonically increasing, i.e., $\Omega_{ij} \leq \Omega_{ik}$ for $j \leq k$. We follow the approach of learning the first-order differences Δ_{ij} between subsequent thresholds, by using softplus for smoothly enforcing positivity ($\text{softplus}(\Delta_{ij}) = \Omega_{ij+1} - \Omega_{ij}$)

$$\Omega_{ij} = \sum_{k \leq j} \text{softplus}(\Delta_{ij}), \quad \text{softplus}(x) = \log(1 + e^x).$$

Differentiable thresholding is obtained by using $\mathbb{1}\{\Omega_{ij} \leq x_j\} \approx \sigma((x_j - \Omega_{ij})/\rho)$, where $\rho \geq 0$ is a temperature parameter controlling smoothness. Similar to Eq. (9), we can introduce Gumbel noise to stabilize the training process, since hard thresholds are computed during inference.

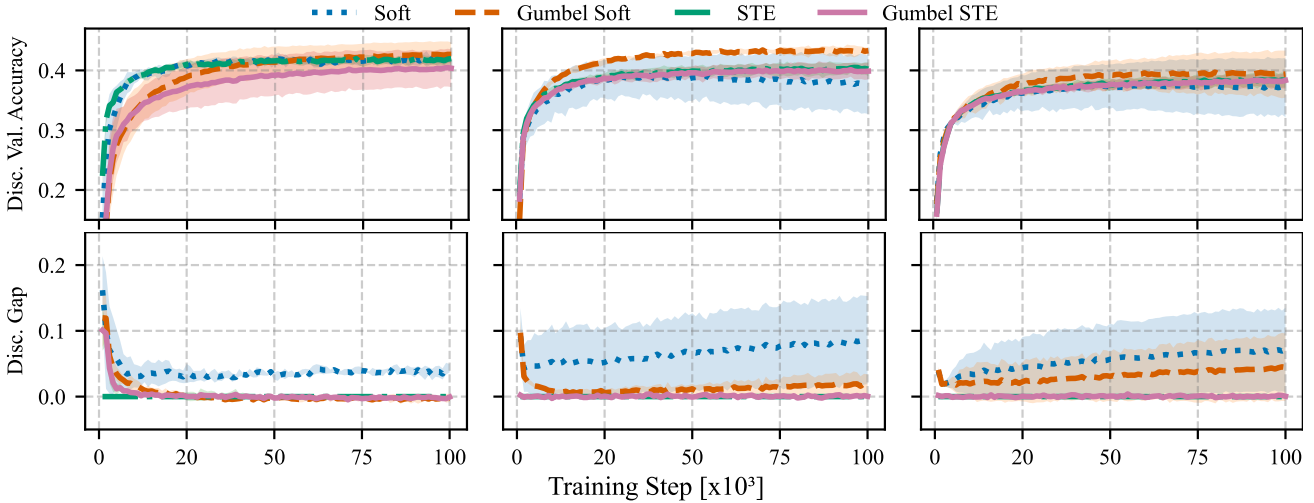


Figure 3. Discrete validation accuracy (top) and discretization gap (bottom) for WARP on CIFAR-10 comparing different parametrization methods and varying LUT sizes, $n = 2$ (left), $n = 4$ (middle) and $n = 6$ (right).

5. Experiments

We conduct three sets of experiments. First, we highlight the training dynamics of WARP LNNs and show the improving effect of our proposed residual initialization and stochastic smoothing. Secondly, we show the effect of learnable thresholding and that it is not restricted to WARP, but is usable for other LNNs benefiting from continuous inputs. Lastly, the performance of WARP is assessed in comparison to state-of-the-art methods from the literature.

5.1. Training Dynamics

We aim to analyze the training and inference performance of WARP with using different input-arithes for every single neuron. For this, we evaluate model performance on the CIFAR-10 dataset following standard pre-processing and an 80/20 split in training / validation data. The architectures of the models used are shown in Tab. 1. We adopt the ‘‘small’’ model architecture introduced in the original DLGN paper (Petersen et al., 2022) as the baseline and initialize the connections between neurons randomly. Training is done with residual weight initialization and averaged over 5 different seeds with indicating 95% confidence intervals.

In Fig. 3, we compare LUT sizes of $n = 2, 4, 6$ (from left to right) while varying four different methods for training process. Soft refers to the proposed vanilla neuron parametrization in Eq. (7), while Gumbel Soft introduces stochastic smoothing via Eq. (9). Further, we also compare corresponding straight-through estimators (STE) by discretizing the inputs and relaxed parametrizations in the forward pass. Moreover, to obtain intercomparability between different LUT sizes, we reduce the number of neurons for increasing LUT size proportional to their fraction, that is a reduction

of $2 \times$ for $n = 4$ and $3 \times$ for $n = 6$. This leads to the same number of total connections, hinting towards possible deployment advantages for larger LUT sizes on logic-based hardware. Further hyperparameters can be found in Sec. D.

The upper plot panel shows the discrete validation accuracy during training, indicating that different LUT sizes show similar performance. Even though the accuracy is slightly lower for $n = 6$, we stress that we do not aim to obtain optimal performance in this experiment. Rather than fine-tuning the temperature parameter τ , we emphasize that this result already demonstrates that WARP can be scaled to logic blocks with more than two inputs.

As is evident from the bottom plot panel, stochastic smoothing by injecting Gumbel noise reduces the discretization gap, defined as the difference of the relaxed validation accuracy and the discrete validation accuracy. While it is constantly 0 for the STEs, Gumbel Soft is able to reduce the gap by smoothing the optimization landscape. Even though Soft has the best relaxed validation accuracy performance, the discretization gap starts to increase with more training steps, especially for larger LUT sizes. Similar effects are observed for different datasets, architectures and hyperparameter configurations, as is evident from Sec. D.

5.2. Learnable Thresholding

Next, we investigate the effect of learnable thresholding. This is particularly relevant for datasets with heterogeneous feature distributions, where fixed binarization schemes may be suboptimal. To this end, we evaluate different thresholding strategies on the JSC dataset, which exhibits features with varying value ranges and densities.

We adopt the *sm* architecture proposed in (Bacellar et al.,

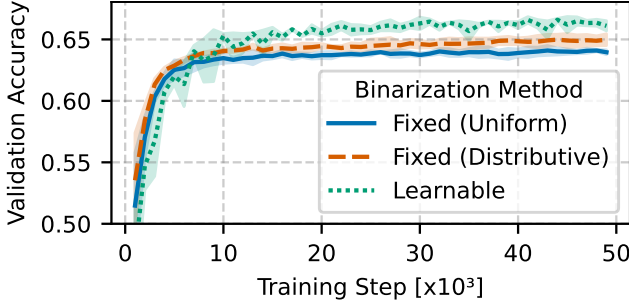


Figure 4. Validation accuracy on CIFAR-10 for different binarization methods. The model architecture resembles LogicTreeNet-M, and the DLGN parametrization according to Eq. (1). Each learning curve consists of three runs with different random seeds.

2024), consisting of two layers with 6-input LUTs, with learnable connections between the input features and the first layer. We compare three different thresholding schemes: (i) fixed uniform thresholds, (ii) fixed distributive thresholds, and (iii) learnable thresholds, which are optimized jointly with the model parameters during training.

The fixed uniform thresholds are placed at equidistant intervals between the minimum and maximum value of each feature. In contrast, distributive thresholding follows the approach of DWN (Bacellar et al., 2024), where thresholds are chosen according to the empirical feature distributions. Learnable thresholding initializes thresholds in the same way, but allows them to adapt during training via gradient-based optimization.

Fig. 5 shows the best validation accuracy on the JSC dataset over 10 training runs with different random seeds, plotted as a function of the number of bits per feature for the binarization. We observe that distributive thresholding already provides a substantial performance improvement over uniform thresholding, which also exhibits the highest variance across runs. Learnable thresholding further improves performance, consistently outperforming distributive thresholding in the low bit-width regime. While distributive thresholding requires approximately 20 bits per feature to reach peak performance, learnable thresholding achieves a comparable accuracy of roughly 70% with only 5 bits. Note that (Bacellar et al., 2024) deploys a 200 bit binarization scheme.

We found the impact of learnable thresholding in the absence of learnable input connections less pronounced, but still significant. Although learnable thresholding is best suited for datasets with strongly varying feature statistics, we additionally evaluate its effect on image data from CIFAR-10. For this experiment, we employ the LogicTreeNet-M architecture and the corresponding parametrization from DLGN (Petersen et al., 2024). In the original work, each pixel is encoded as two bits per color channel, using the fixed uniform thresholding. Fig. 4 depicts the average training curves over

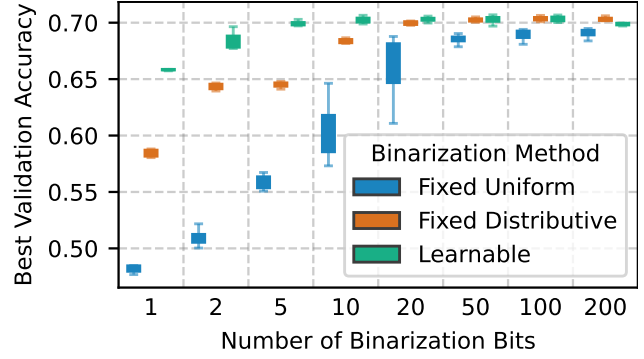


Figure 5. Validation accuracy on JSC for different binarization methods vs the number of bits for the binarization of each feature. The models’ architectures resemble DWN($n=6, sm$) with learnable connections in the first layer. Each configuration was run with ten different random seeds.

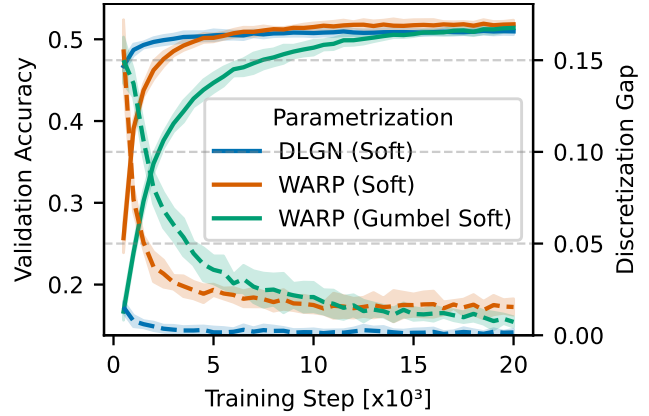


Figure 6. Validation accuracy on CIFAR-10 for a small model with a single convolutional layer. The convolution kernels are implemented as binary trees of depth four and four-input trees of depth two for DLGN, and WARP, respectively.

three runs for all three thresholding strategies. Once again, learnable thresholding yields a significant improvement in final accuracy, albeit with slightly reduced training stability compared to fixed schemes.

In this setting, the two thresholds are learned globally, i.e., shared across all pixels and channels. We also experimented with channel-wise and pixel-wise learnable thresholds but found the increased hyperparameter sensitivity and reduced training stability to outweigh the potential performance gains. A complete list of hyperparameters and training settings is provided in Tab. 4.

5.3. Higher-Rank LUTs in Convolutional Kernels

We investigate the effect of employing higher-rank LUTs within convolutional kernels using WARP. Recall that in DLGN, convolutional kernels with 2^d inputs are implemented as binary trees of depth d , which cannot represent all Boolean functions over its 2^d inputs.

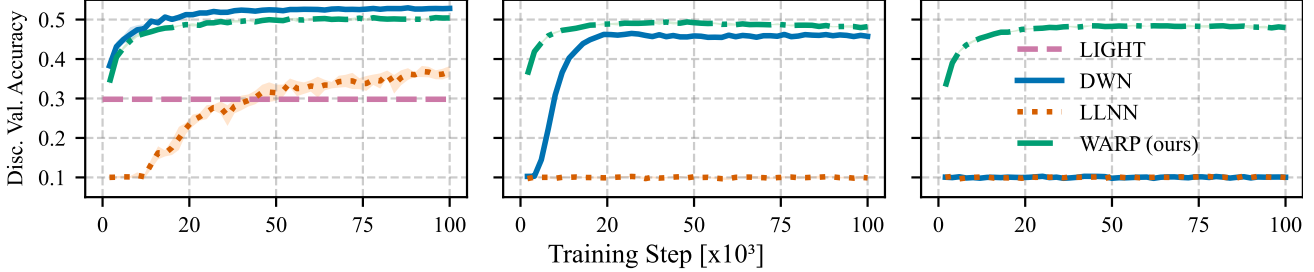


Figure 7. Discrete validation accuracy (top) for DWN (Bacellar et al., 2024), LLNN (Ramírez et al., 2025), LIGHT (Rüttgers et al., 2025) and WARP (ours) on CIFAR-10 with a deep architecture comparing varying LUT sizes, $n = 2$ (left), $n = 4$ (middle) and $n = 6$ (right).

Using WARP, we instead construct convolutional kernels from higher-input LUTs. Specifically, we implement kernels composed of 4-input LUTs arranged in a tree of depth $d = 2$, resulting in an effective receptive field of 4^2 inputs. We compare this configuration to a DLGN kernel with a binary tree depth of $d = 4$, which aggregates 2^4 inputs per kernel.

Despite having the same number of inputs, the two approaches differ in parameter count: A DLGN kernel with depth 4 requires $16 \cdot (8+4+2+1)$ trainable parameters, whereas the corresponding WARP kernel requires only $16 \cdot (4+1)$ parameters. Moreover, the evaluation of trees is fundamentally sequential and cannot be parallelized, hence the shallower WARP tree reduces the number of required sequential operations. As a result, WARP kernels provide higher expressive power with fewer parameters and improved parallelism.

Fig. 6 compares these two kernel implementations on CIFAR-10. We employ a small model consisting of a single convolutional layer with a skip connection, which combines its output with the previous layer using a relaxed OR operation. All remaining dense connections in the network are implemented using logic gates, such that only the convolutional kernel construction differs between the two models. The architecture is described in more detail in Tab. 2.

The results show that WARP kernels with higher-input LUTs achieve slightly higher final discrete accuracy than the DLGN baseline. However, this improvement comes at the cost of slower convergence during training, indicating a trade-off between expressivity and optimization difficulty when increasing LUT-arity in convolutional settings. We attribute the slower convergence to the increased discretization gap, which currently prevents this approach from efficiently scaling to deeper architectures such those in Fig. 4.

5.4. Comparison to n -LUT State-of-the-Art

We show the advantages of WARP over other fully expressive LNNs from the literature. For comparison, we analyze the scalability of DWNs (Bacellar et al., 2024), LLNNs (Ramírez et al., 2025) and LIGHT (Rüttgers et al.,

2025) by considering a deep version of the medium-sized model architecture from (Petersen et al., 2022) for CIFAR-10. Following (Rüttgers et al., 2025), we introduce a depth factor D that scales the number of layers in the network.

In Fig. 7, we plot the learning curves with respect to the discrete validation accuracy for $n=2,4,6$ (left to right) and $D = 3$. We observe that DWN still performs well for $n = 2$ but its performance strongly degrades for higher LUT ranks. This is due to the usage of approximate gradients hindering scalability to larger architectures. Unfortunately, the code for LIGHT is not available. Since results are only reported for $n = 2$, we fall back on reporting approximate numbers stated in the paper. We observe that WARP strongly outperforms LIGHT, with reaching a higher accuracy. Comparing to LLNN, we can see that WARP exhibits better convergence due to the proposed residual initialization for $n = 2$, while LLNN completely fails to learn for $n=4,6$.

6. Conclusion

We introduced WARP, a differentiable and parameter-efficient framework for learning logic neural networks based on the Walsh–Hadamard transform. WARP provides a fully expressive parametrization of Boolean functions while avoiding the redundancy, approximation errors, and scalability limitations of prior approaches. Through learnable thresholding, residual initialization, and stochastic smoothing, WARP enables stable training and significantly faster convergence, while narrowing the gap between relaxed training and discrete logic inference. Our experiments demonstrate that WARP scales effectively to deeper architectures and higher-arity logic blocks, making it a promising foundation for efficient, hardware-native inference.

While we do not report results on hardware deployment, we expect performance at least on par with existing methods, since WARP learns equivalent logic structures. In future work, we plan to evaluate WARP on hardware targets to quantify inference latency and resource utilization, and to benchmark performance on larger-scale datasets.

Impact Statement

This paper presents work whose goal is to advance the field of Machine Learning. There are many potential societal consequences of our work, none which we feel must be specifically highlighted here.

Acknowledgments

This work was supported by the National Science Foundation under Cooperative Agreement PHY-2323298.

References

Aarrestad, T., Loncar, V., Ghielmetti, N., Pierini, M., Summers, S., Ngadiuba, J., Petersson, C., Linander, H., Iiyama, Y., Di Guglielmo, G., Duarte, J., Harris, P., Rankin, D., Jindariani, S., Pedro, K., Tran, N., Liu, M., Kreinar, E., Wu, Z., and Hoang, D. Fast convolutional neural networks on fpgas with hls4ml. *Machine Learning: Science and Technology*, 2(4):045015, July 2021. ISSN 2632-2153. doi: 10.1088/2632-2153/ac0ea1. URL <http://dx.doi.org/10.1088/2632-2153/ac0ea1>.

Aleksander, I., De Gregorio, M., França, F. M. G., Lima, P. M. V., and Morton, H. A brief introduction to weightless neural systems. In *Proceedings of the 17th European Symposium on Artificial Neural Networks (ESANN)*, pp. 299–305, 2009.

Andronic, M. and Constantinides, G. A. Polylut: learning piecewise polynomials for ultra-low latency fpga lut-based inference. In *Proceedings of the 2023 International Conference on Field Programmable Technology (ICFPT)*, pp. 60–68. IEEE, 2023.

Andronic, M. and Constantinides, G. A. Neuralut: Hiding neural network density in boolean synthesizable functions. In *Proceedings of the 34th International Conference on Field-Programmable Logic and Applications (FPL)*, pp. 140–148. IEEE, 2024.

Andronic, M. and Constantinides, G. A. Neuralut-assemble: Hardware-aware assembling of sub-neural networks for efficient lut inference. In *Proceedings of the 33rd IEEE Annual International Symposium on Field-Programmable Custom Computing Machines (FCCM)*, pp. 208–216. IEEE, 2025.

Bacellar, A. T., Susskind, Z., Breternitz, M., John, E., John, L. K., Lima, P. M., França, F. M., et al. Differentiable weightless neural networks. In *Proceedings of the 41st International Conference on Machine Learning, PMLR*, volume 235, pp. 2277–2295, 2024.

Bacellar, A. T., Jadhao, M. P., Nag, S., Lima, P., Franca, F. M., and John, L. K. nanoml for human activity recognition. *arXiv preprint arXiv:2502.12173*, 2025.

Bhat, M. N., Russo, M., Carloni, L. P., Di Guglielmo, G., Fahim, F., Li, A. C., and Perdue, G. N. Machine learning for arbitrary single-qubit rotations on an embedded device. *Quantum Machine Intelligence*, 7(1):8, 2025.

Carneiro, H. C., Pedreira, C. E., França, F. M., and Lima, P. M. The exact vc dimension of the wisard n-tuple classifier. *Neural computation*, 31(1):176–207, 2019.

Chen, H., Wang, Y., Xu, C., Shi, B., Xu, C., Tian, Q., and Xu, C. Addernet: Do we really need multiplications in deep learning? In *Proceedings of the 2020 IEEE/CVF Conference on Computer Vision and Pattern Recognition (CVPR)*, pp. 1468–1477, 2020.

Chmiel, B., Ben-Uri, L., Shkolnik, M., Hoffer, E., Banner, R., and Soudry, D. Neural gradients are near-lognormal: improved quantized and sparse training. In *Proceedings of the 9th International Conference on Learning Representations (ICLR)*, 2021.

Elhoushi, M., Chen, Z., Shafiq, F., Tian, Y. H., and Li, J. Y. Deepshift: Towards multiplication-less neural networks. In *Proceedings of the 2021 IEEE/CVF Conference on Computer Vision and Pattern Recognition (CVPR)*, pp. 2359–2368, 2021.

Fino and Algazi. Unified matrix treatment of the fast walsh-hadamard transform. *IEEE Transactions on Computers*, 100(11):1142–1146, 1976.

Gholami, A., Kim, S., Dong, Z., Yao, Z., Mahoney, M. W., and Keutzer, K. A survey of quantization methods for efficient neural network inference. In *Low-Power Computer Vision*, pp. 291–326. Chapman and Hall/CRC, 2022.

He, K., Zhang, X., Ren, S., and Sun, J. Deep residual learning for image recognition. In *Proceedings of the IEEE conference on computer vision and pattern recognition*, pp. 770–778, 2016.

Hedayat, A. and Wallis, W. D. Hadamard matrices and their applications. *The annals of statistics*, pp. 1184–1238, 1978.

Hellerstein, L. and Servedio, R. A. On pac learning algorithms for rich boolean function classes. *Theoretical Computer Science*, 384(1):66–76, 2007.

Hoang, D., Gupta, A., and Harris, P. Kanel\’e: Kolmogorov-arnold networks for efficient lut-based evaluation. *arXiv preprint arXiv:2512.12850*, 2025.

Hoefler, T., Alistarh, D., Ben-Nun, T., Dryden, N., and Peste, A. Sparsity in deep learning: Pruning and growth for efficient inference and training in neural networks. *Journal of Machine Learning Research*, 22(241):1–124, 2021.

Hubara, I., Courbariaux, M., Soudry, D., El-Yaniv, R., and Bengio, Y. Binarized neural networks. *Advances in neural information processing systems*, 29, 2016.

Jang, E., Gu, S., and Poole, B. Categorical reparameterization with gumbel-softmax. In *Proceedings of the 5th International Conference on Learning Representations (ICLR)*, 2017.

Khataei, A. and Bazargan, K. Treelut: An efficient alternative to deep neural networks for inference acceleration using gradient boosted decision trees. In *Proceedings of the 2025 ACM/SIGDA International Symposium on Field Programmable Gate Arrays (FPGA)*, pp. 14–24, 2025.

Kim, Y. Deep stochastic logic gate networks. *IEEE Access*, 11:122488–122501, 2023.

Kresse, F., Yu, E., and Lampert, C. H. Scalable interconnect learning in boolean networks. *arXiv preprint arXiv:2507.02585*, 2025.

Kunz. On the equivalence between one-dimensional discrete walsh-hadamard and multidimensional discrete fourier transforms. *IEEE Transactions on Computers*, 100(3): 267–268, 1979.

LeCun, Y., Bengio, Y., and Hinton, G. Deep learning. *Nature*, 521(7553):436–444, 2015.

Lin, S., Ji, R., Li, Y., Wu, Y., Huang, F., and Zhang, B. Accelerating convolutional networks via global & dynamic filter pruning. In *Proceedings of the 27th International Joint Conference on Artificial Intelligence (IJCAI)*, volume 2, pp. 8. Stockholm, 2018.

Liu, S., Chen, T., Chen, X., Shen, L., Mocanu, D. C., Wang, Z., and Pechenizkiy, M. The unreasonable effectiveness of random pruning: Return of the most naive baseline for sparse training. In *Proceedings of the 10th International Conference on Learning Representations (ICLR)*. OpenReview, 2022.

Maddison, C., Mnih, A., and Teh, Y. The concrete distribution: A continuous relaxation of discrete random variables. In *Proceedings of the 5th International Conference on Learning Representations (ICLR)*. International Conference on Learning Representations, 2017.

Martins, A., Lopez, M., Baltus, G., Meijer, Q., van der Sluys, M., Van Den Broeck, C., and Caudill, S. Improving early detection of gravitational waves from binary neutron stars using cnns and fpgas. *Machine Learning: Science and Technology*, 6(1):015072, 2025.

Mommen, W., Keuninckx, L., Hartmann, M., and Wambacq, P. A method for optimizing connections in differentiable logic gate networks. *arXiv preprint arXiv:2507.06173*, 2025.

Nguyen, V. M., Ocampo-Blandon, C., Askri, A., Leconte, L., and Tran, B.-H. Bold: Boolean logic deep learning. *Advances in Neural Information Processing Systems*, 37: 61912–61962, 2024.

O’Donnell, R. *Analysis of boolean functions*. Cambridge University Press, 2014.

Petersen, F., Borgelt, C., Kuehne, H., and Deussen, O. Deep differentiable logic gate networks. *Advances in Neural Information Processing Systems*, 35:2006–2018, 2022.

Petersen, F., Kuehne, H., Borgelt, C., Welzel, J., and Ermon, S. Convolutional differentiable logic gate networks. *Advances in Neural Information Processing Systems*, 37: 121185–121203, 2024.

Qin, H., Gong, R., Liu, X., Bai, X., Song, J., and Sebe, N. Binary neural networks: A survey. *Pattern Recognition*, 105:107281, 2020.

Ramírez, I., Garcia-Espinosa, F. J., Concha, D., Aranda, L. A., and Schiavi, E. Llnn: A scalable lut-based logic neural network architecture for fpgas. *IEEE Transactions on Circuits and Systems I: Regular Papers*, 2025.

Rüttgers, L., Aczel, T., Plesner, A., and Wattenhofer, R. Light differentiable logic gate networks. *arXiv preprint arXiv:2510.03250*, 2025.

Sun, C., Årrestad, T. K., Loncar, V., Ngadiuba, J., and Spiropulu, M. Gradient-based automatic mixed precision quantization for neural networks on-chip. *arXiv preprint arXiv:2405.00645*, 2024.

Sung, Y.-L., Nair, V., and Raffel, C. A. Training neural networks with fixed sparse masks. *Advances in Neural Information Processing Systems*, 34:24193–24205, 2021.

Susskind, Z., Arora, A., Miranda, I. D., Villon, L. A., Katopodis, R. F., De Araújo, L. S., Dutra, D. L., Lima, P. M., França, F. M., Breternitz Jr, M., et al. Weightless neural networks for efficient edge inference. In *Proceedings of the 31st International Conference on Parallel Architectures and Compilation Techniques (PACT)*, pp. 279–290, 2022.

Susskind, Z., Arora, A., Miranda, I. D., Bacellar, A. T., Villon, L. A., Katopodis, R. F., De Araújo, L. S., Dutra, D. L.,

Lima, P. M., França, F. M., et al. Uleen: A novel architecture for ultra-low-energy edge neural networks. *Transactions on Architecture and Code Optimization (TACO)*, 20(4):1–24, 2023.

Weng, O., Andronic, M., Zuberi, D., Chen, J., Geniesse, C., Constantinides, G. A., Tran, N., Fraser, N. J., Duarte, J. M., and Kastner, R. Greater than the sum of its lut: Scaling up lut-based neural networks with amigolut. In *Proceedings of the 2025 ACM/SIGDA International Symposium on Field Programmable Gate Arrays*, pp. 25–35, 2025.

Yousefi, S., Plesner, A., Aczel, T., and Wattenhofer, R. Mind the gap: Removing the discretization gap in differentiable logic gate networks. *arXiv preprint arXiv:2506.07500*, 2025.

Yue, C. and Jha, N. K. Learning interpretable differentiable logic networks. *IEEE Transactions on Circuits and Systems for Artificial Intelligence*, 2024.

Table 1. Densely connected architectures for JSC, MNIST, FashionMNIST and CIFAR-10 datasets.

Dataset	Model	Layers	Neurons/layer	#Parameters	GroupSum temp
JSC	<i>sm</i>	1	50	3200	1/0.3
MNIST	small	6	6000	48000	1/0.1
FashionMNIST	small	6	6000	48000	1/0.1
CIFAR-10	small	4	12000	48000	1/0.01
	medium	4	128000	512000	1/0.01

 Table 2. Architecture of the **CLGN CIFAR-10 Res** model ($k_{\text{num}} = 32, n_{\text{bits}} = 3$).

Layer	Input dimension	Output dimension	Description
ResidualLogicBlock (DLGN)	$3n_{\text{bits}} \times 32 \times 32$	$2k_{\text{num}} \times 16 \times 16$	Depth = 4, receptive field 3×3 , padding 1
ResidualLogicBlock (WARP)	$3n_{\text{bits}} \times 32 \times 32$	$2k_{\text{num}} \times 16 \times 16$	Depth = 2, receptive field 3×3 , padding 1
Flatten	$2k_{\text{num}} \times 16 \times 16$	$256 \times 2k_{\text{num}}$	Spatial flattening of logic feature maps
LogicDense ₁	$256 \times 2k_{\text{num}}$	$512k_{\text{num}}$	Fully connected logic layer
LogicDense ₂	$512k_{\text{num}}$	$256k_{\text{num}}$	Fully connected logic layer
LogicDense ₃	$256k_{\text{num}}$	$320k_{\text{num}}$	Fully connected logic layer
GroupSum	$320k_{\text{num}}$	10	Grouped logic aggregation with temperature τ

 Table 3. The 16 Boolean functions of two inputs, sorted lexicographically by their truth tables (ordered as 00, 01, 10, 11), with probabilistic surrogates, WH coefficients $(\gamma_1, \gamma_2, \gamma_3, \gamma_4)$ and indicator coefficients $(\beta_1, \beta_2, \beta_3, \beta_4)$.

#	Gate	Formula	00	01	10	11	Surrogate	WH	Indicator	Icon
1	CONST0	0	0	0	0	0	0	(1, 0, 0, 0)	(0, 0, 0, 0)	
2	AND	$a \wedge b$	0	0	0	1	ab	$(\frac{1}{2}, \frac{1}{2}, \frac{1}{2}, -\frac{1}{2})$	(0, 0, 0, 1)	
3	$a \wedge \neg b$	$a \wedge \neg b$	0	0	1	0	$a(1 - b)$	$(\frac{1}{2}, -\frac{1}{2}, \frac{1}{2}, \frac{1}{2})$	(0, 0, 1, 0)	
4	$\text{ID}(a)$	a	0	0	1	1	a	(0, 0, 1, 0)	(0, 0, 1, 1)	
5	$\neg a \wedge b$	$\neg a \wedge b$	0	1	0	0	$(1 - a)b$	$(\frac{1}{2}, \frac{1}{2}, -\frac{1}{2}, \frac{1}{2})$	(0, 1, 0, 0)	
6	$\text{ID}(b)$	b	0	1	0	1	b	(0, 1, 0, 0)	(0, 1, 0, 1)	
7	XOR	$a \oplus b$	0	1	1	0	$a + b - 2ab$	(0, 0, 0, 1)	(0, 1, 1, 0)	
8	OR	$a \vee b$	0	1	1	1	$a + b - ab$	$(-\frac{1}{2}, \frac{1}{2}, \frac{1}{2}, \frac{1}{2})$	(0, 1, 1, 1)	
9	NOR	$\neg(a \vee b)$	1	0	0	0	$1 - a - b + ab$	$(\frac{1}{2}, -\frac{1}{2}, -\frac{1}{2}, -\frac{1}{2})$	(1, 0, 0, 0)	
10	XNOR	$\neg(a \oplus b)$	1	0	0	1	$1 - a - b + 2ab$	(0, 0, 0, -1)	(1, 0, 0, 1)	
11	NOT(b)	$\neg b$	1	0	1	0	$1 - b$	(0, -1, 0, 0)	(1, 0, 1, 0)	
12	$\text{IMP}(b \rightarrow a)$	$\neg b \vee a$	1	0	1	1	$1 - b + ab$	$(-\frac{1}{2}, -\frac{1}{2}, \frac{1}{2}, -\frac{1}{2})$	(1, 0, 1, 1)	
13	NOT(a)	$\neg a$	1	1	0	0	$1 - a$	(0, 0, -1, 0)	(1, 1, 0, 0)	
14	$\text{IMP}(a \rightarrow b)$	$\neg a \vee b$	1	1	0	1	$1 - a + ab$	$(-\frac{1}{2}, \frac{1}{2}, -\frac{1}{2}, -\frac{1}{2})$	(1, 1, 0, 1)	
15	NAND	$\neg(a \wedge b)$	1	1	1	0	$1 - ab$	$(-\frac{1}{2}, -\frac{1}{2}, -\frac{1}{2}, \frac{1}{2})$	(1, 1, 1, 0)	
16	CONST1	1	1	1	1	1	1	(-1, 0, 0, 0)	(1, 1, 1, 1)	

A. Generality of WARP

Proof. We proof Theorem 4.1.

WARP is Most Parameter Efficient First, we remark that ϕ_i^W is an orthonormal basis for all functions $g : \{-1, 1\}^n \rightarrow \{-1, 1\}$

$$g(\mathbf{s}) = \sum_{i \in [2^n]} \theta_i \phi_i^W(\mathbf{s}), \quad \langle \phi_i^W, \phi_j^W \rangle = \sum_{\mathbf{s} \in \{-1, 1\}^n} \phi_i^W(\mathbf{s}) \phi_j^W(\mathbf{s}) = \sum_{k \in [2^n]} H_{ik} H_{kj} = \delta_{ij}.$$

Through orthogonality, it follows that the rows of \mathbf{H} are linearly independent which leads to the orthonormal basis argument. Thus, no other parametrization exists that can represent every g with less parameters.

WARP is More General Than LLNN A basis change w.r.t. ϕ_i^1 can be computed by finding a basis transformation matrix \mathbf{T} with

$$T_{ij} = \langle \phi_i^1, \phi_j^W \rangle = \sum_{s \in \{-1, 1\}^n} \mathbb{1}_{\mathbf{b}^{(i)}}(\varphi^{-1}(s)) \phi_j^W(s) = \sum_{k \in [2^n]} \delta_{ik} H_{kj} = H_{ij}.$$

Thus, any $s \in \{-1, 1\}^n$ can be transformed between the bases by using the Hadamard matrix $\sum_{ij} H_{ij} \phi_j^W(s) = \phi_i^1(s)$. While the LLNN parametrization restricts their parameters to be in $[0, 1]$ through applying the sigmoid function, WARP allows them to take arbitrary values in \mathbb{R} . \square

WARP is More General Than DWN In fact, the DWN parametrization is similar to LLNN, but uses a straight-through estimator in the forward pass

$$f_{\text{DWN}}(\mathbf{x}) = \varphi(f_{\text{LLNN}}(\varphi^{-1}(\text{sgn}(\mathbf{x})))).$$

Hence, it relies on approximate gradients and is less general than LLNN and through the previous statement, DWN is also less general than WARP by means of a non-bijective mapping sgn .

WARP is Less Redundant and More Parameter-Efficient Than DLGN Even though the the functions $\phi_j^{\text{DLGN}}(s)$ are spanning all Boolean functions, they do not form a basis. DLGNs are parametrized by way more parameters ($2^n \ll 2^{2^n}$) and a linear projection to the LLNN basis is given by

$$\mathbf{P} \in \{0, 1\}^{2^n \times 2^{2^n}}, P_{ij} = b_i^{(j)} \in \{0, 1\} \Rightarrow \sum_{k \in [2^{2^n}]} P_{ij} \phi_j^{\text{DLGN}}(s) = \phi_i^1(s), \forall i \in [2^n].$$

Hence, DLGNs introduce a lot of redundancy.

B. Parametrization Discretization

Proof. We proof Theorem 4.2. The discretization error in the p -norm is given as

$$\|\mathbf{f}_{\text{WARP}} - \mathbf{t}\|_p = \left(\sum_i \left| f(\mathbf{b}^{(i)}) - t_i \right|^p \right)^{\frac{1}{p}}.$$

Finding an optimal discretization strategy $\mathbf{t} \in \{0, 1\}^{2^n}$ leads to

$$\arg \min_{\mathbf{t} \in \{0, 1\}^{2^n}} \|\mathbf{f}_{\text{WARP}} - \mathbf{t}\|_p \Leftrightarrow \arg \min_{t_i \in \{0, 1\}} \left| f(\mathbf{b}^{(i)}) - t_i \right|,$$

for all $i \in [2^n]$ and with

$$t_i^{(f_{\text{WARP}})} = \arg \min_{t \in \{0, 1\}} \left| f(\mathbf{b}^{(i)}) - t \right| = \arg \min_{t \in \{0, 1\}} \left| \sigma \left(\sum_j H_{ij} \theta_j \right) - t \right| = \left(1 + \text{sgn} \left(\sum_j H_{ij} \theta_j \right) \right) / 2$$

we obtain Eq. (8). For a vector $\mathbf{s} \in \{-1, 1\}^{2^n}$, the WH parameters are obtained by $(1/\sqrt{2^n}) \mathbf{H} \mathbf{s}$. Looking at the parameter vector $\boldsymbol{\theta} \in \mathbb{R}^n$

$$\arg \min_{\mathbf{t} \in \{-1, 1\}^n} \left\| \boldsymbol{\theta} - \frac{1}{\sqrt{2^n}} \mathbf{H} \mathbf{t} \right\|_2 = \arg \min_{\mathbf{t} \in \{-1, 1\}^n} \left\| \mathbf{H} \boldsymbol{\theta} - \frac{1}{\sqrt{2^n}} \mathbf{t} \right\|_2 \Leftrightarrow \arg \min_{\mathbf{t} \in \{-1, 1\}^n} \left| \sum_j H_{ij} \theta_j - \frac{1}{\sqrt{2^n}} t_j \right| = \text{sgn} \left(\sum_j H_{ij} \theta_j \right) \forall i \in [2^n],$$

where we used the norm-preserving property of the unitary matrix \mathbf{H} . \square

C. Parameter Initialization

Proof. We proof the validity of the residual intialization in Eq. (10). The LUT of the pass-through function $f(\mathbf{x}) = x_n$ is given by $t_i^{(f)} = 0$ if $i < \ell$ and $t_i^{(f)} = 1$ else with $\ell = 2^{n-1} + 1$. Thus, aiming for the WARP parametrization to represent f with probability p for every LUT entry leads to

$$\begin{aligned} \mathbb{P}(t_i^{(f_{\text{WARP}})} = t_i^{(f)}) = p, \forall i \Leftrightarrow f_{\text{WARP}}(\mathbf{b}^{(i)}) = 1 - p, i < \ell \wedge f_{\text{WARP}}(\mathbf{b}^{(i)}) = p, i \geq \ell \\ \Leftrightarrow \sigma\left(\frac{\sqrt{2^n}}{\tau} \sum_j H_{ij} \theta_j\right) = 1 - p, i < \ell \wedge \sigma\left(\frac{\sqrt{2^n}}{\tau} \sum_j H_{ij} \theta_j\right) = p, i \geq \ell \\ \Leftrightarrow \sum_j H_{ij} \theta_j = -\frac{\tau}{\sqrt{2^n}} \sigma^{-1}(p), i < \ell \wedge \sum_j H_{ij} \theta_j = \frac{\tau}{\sqrt{2^n}} \sigma^{-1}(p), i \geq \ell, \end{aligned}$$

with $\sigma^{-1}(1 - p) = -\sigma^{-1}(p)$. Due to the recursive structure of the Hadamard matrix

$$\mathbf{H}^{(n+1)} = \frac{1}{\sqrt{2}} \begin{pmatrix} \mathbf{H}^{(n)} & \mathbf{H}^{(n)} \\ \mathbf{H}^{(n)} & -\mathbf{H}^{(n)} \end{pmatrix}, \quad \mathbf{H}^{(1)} = \frac{1}{\sqrt{2}} \begin{pmatrix} 1 & 1 \\ 1 & -1 \end{pmatrix},$$

combining the 2^n different linear equations leads to

$$\begin{aligned} \sum_{i < \ell} \sum_j H_{ij} \theta_j &= \frac{2^{n-1}}{\sqrt{2^n}} (\theta_1 + \theta_\ell) = -\frac{\tau}{\sqrt{2^n}} \sigma^{-1}(p) 2^{n-1}, \\ \sum_{i \geq \ell} \sum_j H_{ij} \theta_j &= \frac{2^{n-1}}{\sqrt{2^n}} (\theta_1 - \theta_\ell) = \frac{\tau}{\sqrt{2^n}} \sigma^{-1}(p) 2^{n-1}. \end{aligned}$$

Subtracting these two equations, we obtain $\theta_\ell = \tau \sigma^{-1}(1 - p)$ and $\theta_1 = 0$. Similarly, it follows that $\theta_i = 0, \forall i \in [2^n] \setminus \{\ell\}$. \square

Gradient Stability The entries of the gradient w.r.t. to the input is computed as

$$\frac{\partial f_{\text{WARP}}(\mathbf{x})}{\partial x_i} = \frac{1}{\tau} \sigma' \left(\frac{1}{\tau} \sum_{i \in [2^n]} \theta_i \phi_i^{\text{W}}(\varphi(\mathbf{x})) \right) \cdot \left(\sum_{i \in [2^n]} \theta_i \frac{\partial}{\partial x_i} \phi_i^{\text{W}}(\varphi(\mathbf{x})) \right).$$

The gradient vanishes if one of the two factors is close to 0. For the first factor, we get

$$\sigma' \left(\frac{1}{\tau} \sum_{i \in [2^n]} \theta_i \phi_i^{\text{W}}(\varphi(\mathbf{x})) \right) = \sigma \left(\frac{1}{\tau} \sum_{i \in [2^n]} \theta_i \phi_i^{\text{W}}(\varphi(\mathbf{x})) \right) \cdot \sigma \left(1 - \frac{1}{\tau} \sum_{i \in [2^n]} \theta_i \phi_i^{\text{W}}(\varphi(\mathbf{x})) \right),$$

which is close to 0 if the argument is $\ll 0$ or $\gg 0$. For our RI, we have

$$\sum_{i \in [2^n]} \theta_i \phi_i^{\text{W}}(\varphi(\mathbf{x})) = \theta_\ell \phi_\ell^{\text{W}}(\varphi(\mathbf{x})) = \theta_\ell \prod_{k \in [n]} \varphi(x_k)^{b_k^{(\ell)}} = \theta_\ell \varphi(x_\ell),$$

which can be well controlled if θ_ℓ is not $\ll 0$ or $\gg 0$.

The second factor evaluates to

$$\sum_{i \in [2^n]} \theta_i \frac{\partial}{\partial x_i} \phi_i^{\text{W}}(\varphi(\mathbf{x})) = \theta_\ell \frac{\partial}{\partial x_\ell} \varphi(x_\ell) = -2\theta_\ell,$$

which is also well controlled if θ_ℓ is < 0 or > 0 . Our proposed RI intialization thus prevents gradient vanishing, compared to random initialization (Rüttgers et al., 2025).

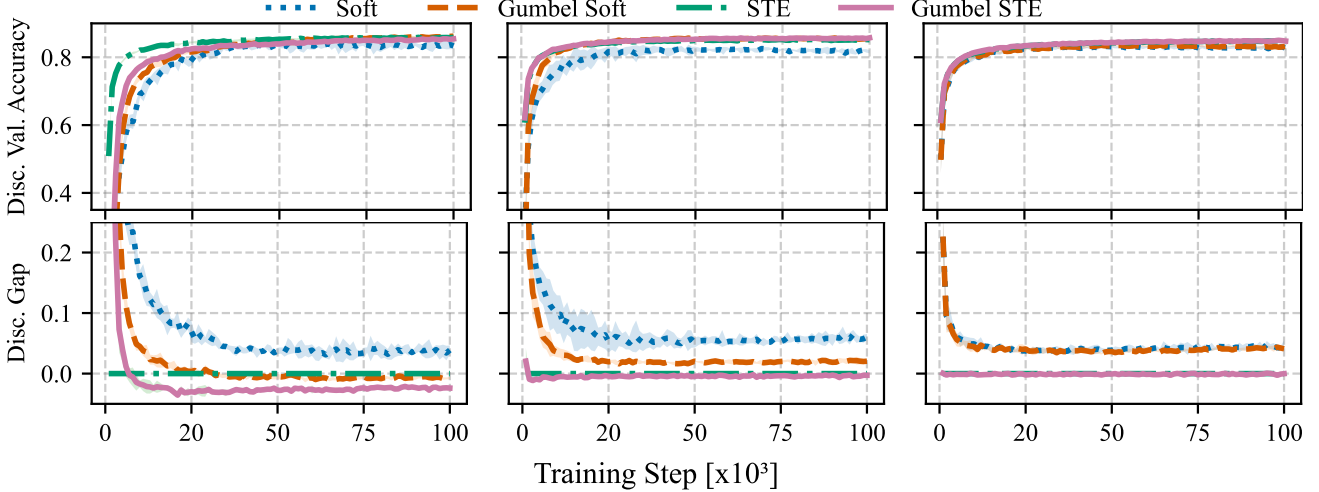


Figure 8. Discrete validation accuracy (top) and discretization gap (bottom) for WARP on FashionMNIST comparing different parametrization methods and varying LUT sizes, $n = 2$ (left), $n = 4$ (middle) and $n = 6$ (right).

Intercomparability to DLGN DLGNs use RI, introducing skip connections by increasing probability of sampling identity gates. Introducing a parameter $c \geq 0$ controlling this increase, we obtain

$$\begin{aligned}
 \mathbb{P}(t_i^{(f_{\text{DLGN}})} = 1) &= f_{\text{DLGN}}(\mathbf{b}^{(i)}) = \sum_j \alpha_j \phi_j^{\text{DLGN}}(\mathbf{b}^{(i)}) \\
 &= \frac{1}{e^c + 2^{2^n} - 1} \sum_j t_i^{(j)} c'_j, \quad c'_j = \begin{cases} e^c, & \text{if } j = 2^{2^{n-1}} - 1, \\ 1, & \text{else.} \end{cases} \\
 &= \frac{1}{e^c + 2^{2^n} - 1} \left(t_i^{(j')} e^c + \sum_{j \neq j'} t_i^{(j)} \right) \\
 &= \frac{1}{e^c + 2^{2^n} - 1} \left(\delta_{i > 2^{n-1}} e^c + 2^{2^{n-1}} - \delta_{i > 2^{n-1}} \right).
 \end{aligned}$$

To obtain intercomparability between methods, we want $\mathbb{P}(t_i^{(f_{\text{DLGN}})} = t_i^{(f)}) = \mathbb{P}(t_i^{(f_{\text{WARP}})} = t_i^{(f)}) = p$. Thus,

$$\theta_\ell = \tau \sigma^{-1} (1 - p) = (2^n - 1) \log(2) - \log \left(e^c + 2^{2^n - 1} - 1 \right).$$

For obtaining the corresponding value of c representing a certain probability p , we compute

$$\begin{aligned}
 \frac{1}{e^c + 2^{2^n} - 1} \left(2^{2^{n-1}} \right) &= 1 - p \\
 \Leftrightarrow e^c + 2^{2^n} - 1 &= \frac{2^{2^{n-1}}}{1 - p} \\
 \Leftrightarrow c &= \left(\frac{2^{2^{n-1}}}{1 - p} - 2^{2^n} + 1 \right).
 \end{aligned}$$

D. Training Dynamics on MNIST and Fashion-MNIST

We run a similar experiment to the one conducted in Sec. 5.1, but on different datasets. That is, we plot the discrete validation accuracy and the discretization gap for LUT sizes $n = 2, 4, 6$ on MNIST and FashionMNIST, varying the parametrization with using Gumbel noise injection and STEs. For both datasets, we utilize the small model from (Petersen et al., 2022) and the plots are given in Figs. 8 and 9. We scale the temperature parameter τ proportional to the number of parameters to accommodate for the number of summands, that is $\tau = 1$ for $n = 2$, $\tau = 4$ for $n = 4$, and $\tau = 16$ for $n = 6$.

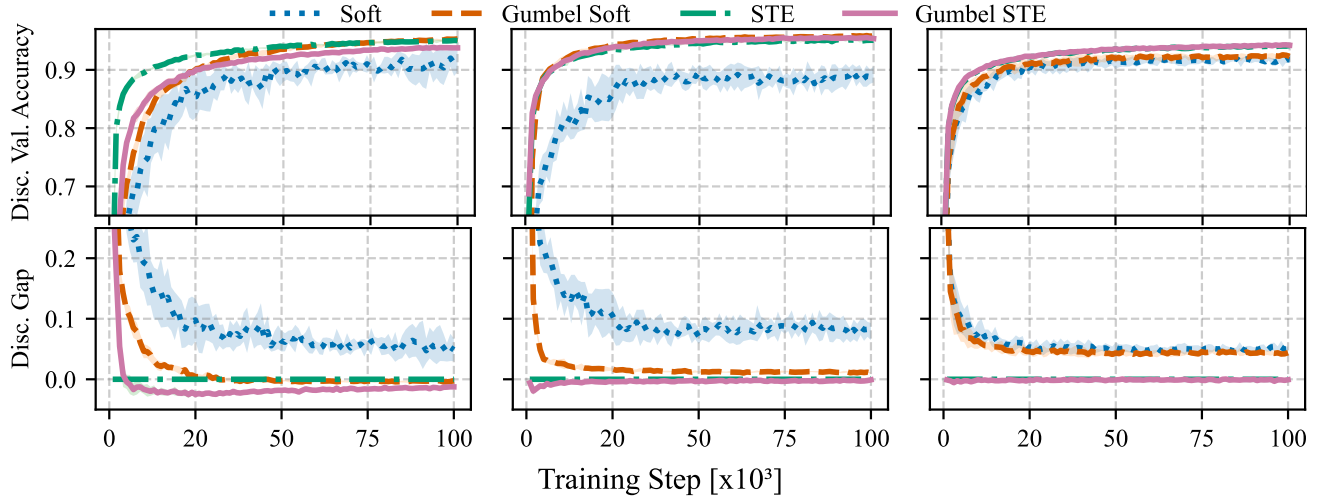


Figure 9. Discrete validation accuracy (top) and discretization gap (bottom) for WARP on MNIST comparing different parametrization methods and varying LUT sizes, $n = 2$ (left), $n = 4$ (middle) and $n = 6$ (right).

Table 4. Hyperparameters used in the thresholding and high-input convolution experiments. Parameters not listed were adopted from the original literature of the respective model architectures.

Experiment	Hyperparameter	Value
Learnable Thresholding (JSC)	Batch size	128
	Forward sampling	Gumbel-Soft
	Learning rate	0.002
	WARP sigmoid temperature	1.0
	Binarization learning rate	$1/n_{\text{bits}}$ (relative)
	Binarization temperature	0.001
	Binarization temperature (Softplus)	0.001
	Residual initialization probability	0.95
Learnable Thresholding (CIFAR-10)	Binarization learning rate	0.02
	Binarization temperature	0.0002
	Binarization temperature (Softplus)	0.01
High-Input Convolutions	Batch size	128
	Parametrization temperature	1.0
	Residual initialization probability	0.95